This paper can be found at DOI: 10.1007/s10853-015-9409-y

Orientation of Cellulose Nanocrystals in Electrospun Polymer Fibres

N.D. Wanasekara[a], R.P.O. Santos[a,b], C. Douch[a], E. Frollini[b], S.J. Eichhorn[a],

a. College of Engineering, Mathematics and Physical Sciences, University of Exeter, Physics building, Stocker Road, Exeter, United Kingdom. EX4 4QL, UK;

b. Macromolecular Materials and Lignocellulosic Fibers Group, Center for Research on Science and Technology of BioResources, Institute of Chemistry of São Carlos, University of São Paulo, 13560-970 São Carlos São Paulo, Brazil

Corresponding author: s.j.eichhorn@exeter.ac.uk; Tel: +44(0)1392 72 5515, Fax: +44(01)1392 21 7965.

Abstract

Polystyrene (PS) and poly(vinyl alcohol) (PVA) nanofibers containing cellulose nanocrystals (CNCs) were successfully produced by electrospinning. Understanding the local orientation of CNCs in electrospun fibres is critical to understand and exploit their mechanical properties. The orientation of CNCs in these electrospun fibres was investigated using Transmission Electron Microscopy (TEM) and Raman spectroscopy. A Raman band located at ~1095 cm^{-1}, associated with the C-O ring stretching of the cellulose backbone, was used to quantify the orientation of the CNCs within the fibres. Raman spectra were fitted using a theoretical model to characterise the extent of orientation. From these data it is shown that the CNCs have little orientation along the direction parallel to the axis of the fibres. Evidence for both oriented and non-oriented regions of CNCs in the fibres are presented from TEM images of nanofibres. These results contradict previously published work in this area and micromechanical modelling calculations suggest a uniform orientation of CNCs in electrospun polymer fibres. It is demonstrated that this explains why the mechanical properties of electrospun fibre mats containing CNCs are not always what would be expected for a fully oriented system.

Introduction

Cellulose is the most abundant biopolymer on earth and exhibits the potential to be reshaped into an array of forms ranging from non-woven paper to high performance fibres [1]. In addition, cellulose offers an attractive alternative to synthetic polymers due its biodegradability, renewability and sustainability. Cellulose in the native state consists of both amorphous and crystalline regions, which can be isolated to form cellulose nanocrystals (CNCs) by a controlled acid hydrolysis process [2]. Cellulose nanocrystals can be derived from a myriad of source materials ranging from cotton to grape skin [3]. CNCs are a potential reinforcement for other polymers due to their high aspect ratio, high elastic modulus (120-150 GPa) and excellent chemical and thermal properties [4]. CNCs have therefore attracted a lot of attention as a reinforcement for thin and functional polymer films [5] and nano- and micro- fibres [6, 7].

CNCs have been utilized as reinforcement in composite nanofibres produced by electrospinning using an array of polymers. Peresin *et al.* [8] successfully electrospun CNC-reinforced poly(vinyl alcohol) fibres with improved morphological and thermomechanical properties. It was shown that increasing the CNC concentration in the fibres led to a significant enhancement of mechanical properties [9]. Electrospun poly(vinyl alcohol) (PVA) fibres have been extensively studied to understand the effects of molecular weight [10], concentration [9] and the presence of additives on mechanical properties and thermal stability [11]. Polystyrene (PS), another commodity polymer, has also been electrospun into fibres [12]. PS exhibits different chemical, phsyical and functional attributes to PVA because of the presence of aromatic groups. Rojas *et al.* [12]

have produced electrospun polystyrene (PS) fibres reinforced with CNCs, observing unique ribbon shapes and the presence of twists along the axes of the fibres. The incorporation of CNCs was found to increase the glassy modulus of the fibres due to their mechanical percolation, forming a stiff and continuous network held together by hydrogen bonding in a hydrophobic matrix environment.

Understanding CNC-polymer interfaces and the orientation of CNCs within electrospun fibres is critical to explain and exploit mechanical properties. Strong matrix-filler interactions lead to efficient stress transfer within composite fibres and oriented CNCs along the fibre axis are expected to enhance anisotropic mechanical properties such as axial stiffness. There have been several studies on directing orientation of different forms of cellulosic materials during processing, via electric fields [13], magnetic fields [14] and conventional wet spinning [15]. However, little work has been published on the orientation of CNCs in fibres produced by electrospinning. Electrospinning is a robust technique of producing networks of composite nanofibres that offer advantages of higher aspect ratios and surface area to suit an array of end applications ranging from biomedical scaffolds to filtration membranes [16]. The possibility of orientating CNCs during electrospinning should be evaluated against the processing conditions and confinement effects. The nano-scale confinement effects resulting from electrospun fibre diameters less than the length of the nanocrystal, may lead to orientation of nanocrystals along the fibre axis direction. In addition, large electrostatic fields, and the orientation of polymer chains during electrospinning, may influence the alignment of cellulose nanocrystals in the fibres.

X-ray diffraction (XRD) and Transmission Electron microscopy (TEM) are the most widely used techniques to assess the orientation of CNCs in fibres. Changsarn *et al.* [17] have utilized TEM to visualize the CNCs embedded within electrospun poly(ethylene oxide) (PEO) fibres of ~100 nm diameter. The absence of any protruding segments from fibres seen in TEM images suggested that the CNCs were indeed oriented along the fibres' axes. Also, they suggest that CNCs are embedded in the core of the electrospun fibre with a high degree of uniaxial alignment. However, they were not able to investigate the orientation of CNC in fibres with larger diameters. Similarly, Raman spectroscopy has been reported as an essential tool in mapping the orientation of CNCs in polymeric matrices [14]; but to date not electrospun fibres. This approach utilizes the measurement of the intensity of a Raman peak related to the nanofiller as a function of rotation of the specimen with respect to the fixed axis of polarization. Using this technique, the polarization direction of the excitation laser is typically parallel to the main orientation direction of the polymer; for fibres this would be along their axes. The intensity of this band remains invariant with rotation angle for nanofillers with random in-plane orientations; however, this intensity changes dramatically for oriented nanofillers e.g. CNCs in a composite [18].

The present work utilizes both TEM and Raman spectroscopy techniques to examine the orientation of CNCs in electrospun fibres of CNC-reinforced poly(vinyl alcohol) and polystyrene. Both TEM images and Raman orientation maps indicate a lack of orientation of CNCs along the fibre axis direction. However, smaller regions with local orientations are found to be present in the fibres. This result contradicts previous work that has suggested uniform orientation of CNCs in electrospun polymer fibres. Some calculations

are given for the predicted mechanical properties of electrospun fibres published in the literature, which based on composite theory applied to the data, are lower than what would be expected for fully oriented systems.

2. Materials and Methods

Freeze dried CNCs were purchased from the Process Development Center at University of Maine. High molecular weight 87-89% hydrolyzed PVA was purchased from Alfa Aesar. Atactic PS with an average molecular weight of ~280,000 determined by GPC was purchased from Sigma Aldrich (Dorset, UK). Dimethylformamide [DMF (purity grade ≥99%)] was purchased from Sigma Aldrich (Dorset, UK) and was used as received.

Aqueous solutions of PVA with varying concentrations of CNCs (10 and 20 wt%) were created as follows. PVA in water was stirred at 80 °C until fully dissolved. Once the PVA solution cooled to room temperature, the CNCs were added and stirred for two days until a homogenously mixed PVA/CNC solution was obtained. The total concentration of PVA in the final solution was 10 (w/v) %. The CNC concentration (10 and 20 wt% of PVA) was calculated relative to the PVA weight in the solution. High wt% values of CNCs were used to ensure a strong signal from the Raman spectrometer emanating from the cellulosic component. Similarly, PS was dissolved in dimethylformamide (DMF) for 24 hours at room temperature to have a concentration of 25% (w/v). Once the PS was fully dissolved, CNCs were added to the solution and stirred for two more days at ambient temperature until homogenously dispersed. These colloidal solutions were then drawn into a syringe, which was attached to a pump in the electrospinning apparatus. Fibres were then

electrospun using the following conditions: flow rate of 1.0 mL/h, 20 kV, 15 cm tip to rotating collector distance (TCD) for PVA/CNC solution and 1.5 mL/h, 15 kV and 10 cm (TCD) for PS/CNC. These conditions produced the best electrospun fibres and they were chosen after trying out a range of spinning conditions. PS/CNC composite fibres were produced using an electrospinning instrument (Electrospinz ES1a) equipped with a custom-built rotating mandrel collector. PVA/CNC composite fibres were produced at a custom–built electrospinning set-up at the Materials Science Centre, University of Manchester. Similar rotational speeds were used to electrospin both PS and PVA fibres though different instruments were used. Once an electrospun mat of fibres was formed, it was removed from the collector.

The PVA and the CNCs are thought to hydrogen bond to each other in the solid state via the primary alcohol groups present on their respective polymer backbones. In the aqueous state CNCs (produced using sulphuric acid) are known to possess negative surface charge due to the presence of sulfate half-ester groups [2]. These aid their dispersion in PVA.

Raman spectra were recorded using a Renishaw 1000 Raman imaging microscope equipped with a thermoelectrically cooled CCD detector. A near-IR laser with a wavelength of 785 nm was used to record spectra from oriented electrospun scaffold samples using an exposure time of 30s and two accumulations. The laser beam was focused using a 40× objective lens onto a few fibres contained within the electrospun mat. Care was taken to focus onto fibres in fully oriented regions of the mats. For orientation mapping experiments, one or a few fibres parallel to the polarization direction of the laser were

chosen. The incident and scattered light radiation was polarized parallel to the principle axis of the Raman spectrometer. The polarization direction of the incident light was rotated using a half-wave plate, and a polarizer was used to maintain the polarization direction of scattered light parallel to the macroscopic orientation direction of the electrospun fibres. The intensities of a Raman band located at ~1095 cm^{-1} were recorded as a function of the rotation angle of the incoming polarizer with respect to the axis of the fibres, and a Lorentzian function was used to fit this Raman peak.

TEM samples were prepared by embedding the electrospun mats in an epoxy resin (TAAB Low Viscosity Resin Hard from TAAB Laboratories Equipment LTD, UK.). These samples were microtomed into thin sections of thickness ~100 nm, both parallel and perpendicular to the fibre axis. Samples were imaged using a TEM (JEM-2100 LaB6) using a voltage of 100 kV.

SEM samples were sputter coated with gold to a thickness of ~10 Å. The samples were imaged using a SEM (HITACHI S3200N SEM-EDS) with a voltage of 20 kV.

3. Results and Discussion

3.1. Orientation and Morphology of Nanofibres

To achieve macroscopic alignment of fibres, a rotating mandrel was utilized as the grounded collector during electrospinning. The orientation of both PVA and PS fibres was found to increase with the rotational speed of the mandrel. We utilized a rotational speed of ~1500 rpm for all the experiments to produce aligned fibres. As shown in Figure 1, the

PS/CNC and PVA/CNC fibres were observed to be oriented parallel to the rotation direction. The fibre surface appeared to be smooth and very few ‘beads’ were observed. Fibre diameter distributions were produced (Figure 2) and they show that the diameters of fibres in the mats have normal distributions. The mean fibre diameters of PS/CNC mats (3.00 ± 0.12 μm for 10% CNCs and 2.83 ± 0.09 μm for 20% CNCs) were significantly higher than the PVA/CNC fibre mats (0.29 ± 0.01 μm for 10% CNCs and 0.36 ± 0.01 μm for 20% CNCs). These differences in fibre diameter can be attributed to the differences in electrospinning conditions, solvents, chemical structures and tacticity of the polymers used. Either single fibres or electrospun oriented fibres were deemed necessary for Raman analysis since filament axes needed to be placed parallel to the polarization direction of the laser. Attempts to obtain isolated single fibres were unsuccessful and thus oriented fibres were utilized for analysis under the Raman spectrometer.

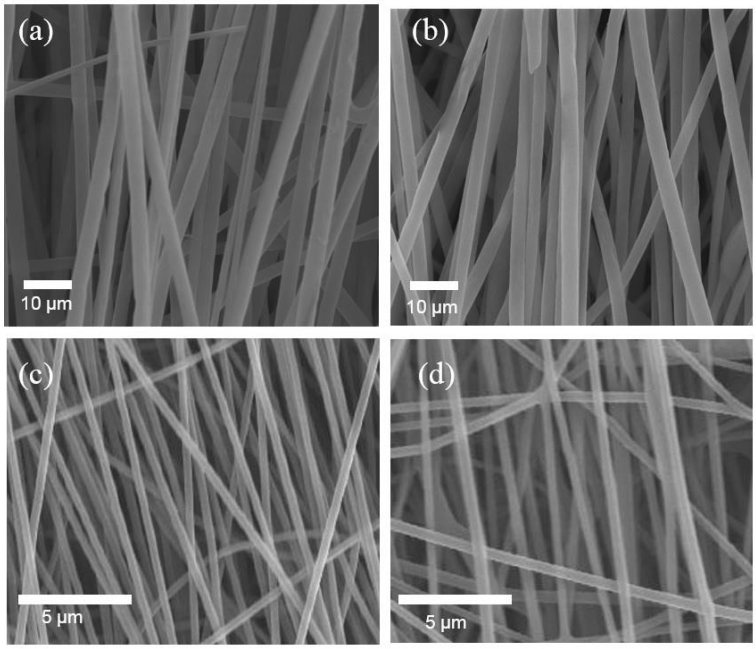

Figure 1. SEM images of oriented fibres of PS/CNC (a) 10% (b) 20%, and PVA/CNC (c) 10% (d) 20%.

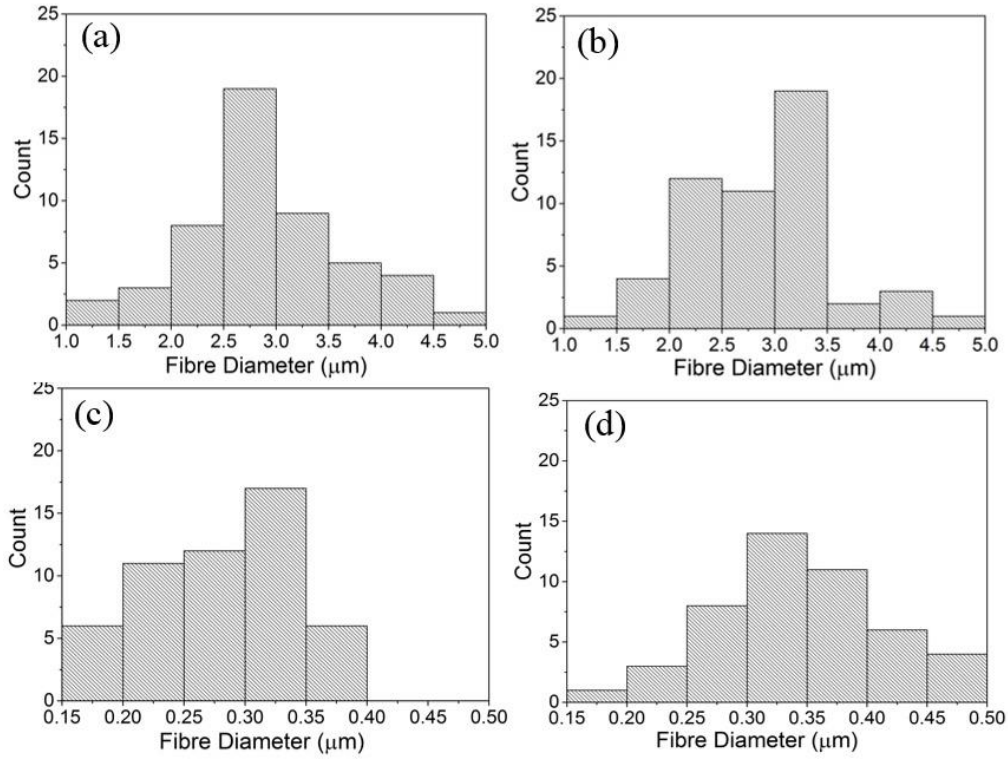

Figure 2. Fibre diameter histograms for PS/CNC (a) 10%, (b) 20% and PS/CNC (c) 10%, (d) 20%

3.2. Raman Spectroscopic Characterization of CNC Orientation

Raman spectra of CNC-reinforced PVA and PS fibres are shown in Figure 3. A Raman peak characteristic of cellulose (and not present for either pure PS or PVA) is located at ~1095 cm^{-1}. This peak can be clearly observed in nanocomposite fibres with 10 and 20 wt.% of CNCs; below this CNC concentration we were not able to observe CNCs. The Raman laser spot size of 1-2 μm was focused on one or two fibres in a PS/CNC mat and a few fibres in PVA/CNC electrospun mats. There may be a small error involved in the measurements on the PVA/CNC sample due to a few fibres possibly lying in directions

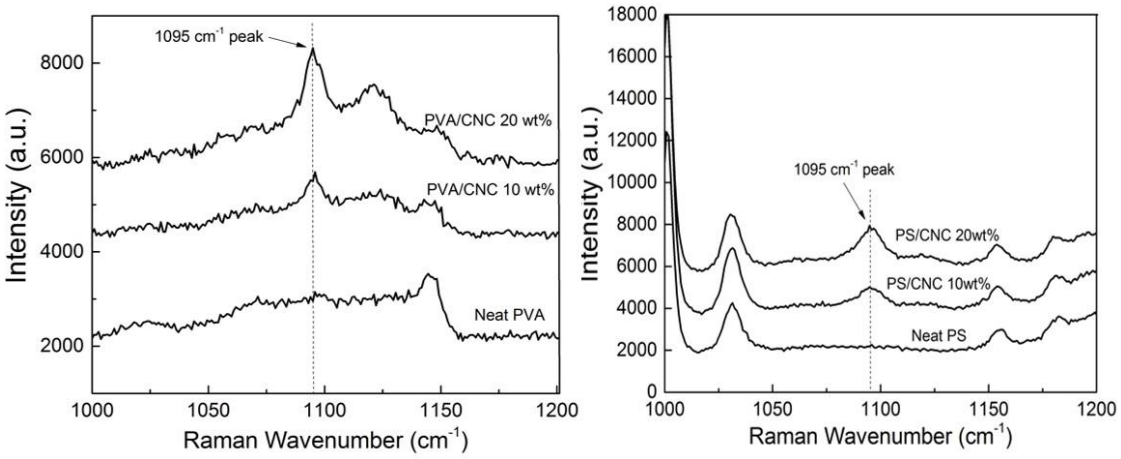

Figure 3. Typical Raman spectra of (left) PVA/CNC (right) PS/CNC.

(Figure 1c & 1d) other than the polarization direction of the laser. The intensity of the Raman peak located at ~1095 cm^{-1} is found to increase with an increase in the CNC concentration. For orientation mapping experiments, the oriented fibre mat was placed under the lens of the Raman microscope in such a way that the polarization of the incident laser was parallel to the longitudinal axis of either a single fibre or a group of aligned fibres. The scattered radiation was sent through a parallel polarization filter. The intensity of the Raman band located at ~1095 cm^{-1} was recorded as a function of rotation angle (0 to 360°). The most intense peak recorded was fitted with a Lorentzian function to determine the maximum intensity from which a normalization of other intensities was performed. As shown in Figure 4, polar plots of the intensity as a function of the rotational angle are presented for the evaluation of the orientation of CNCs in the fibres. The Raman band

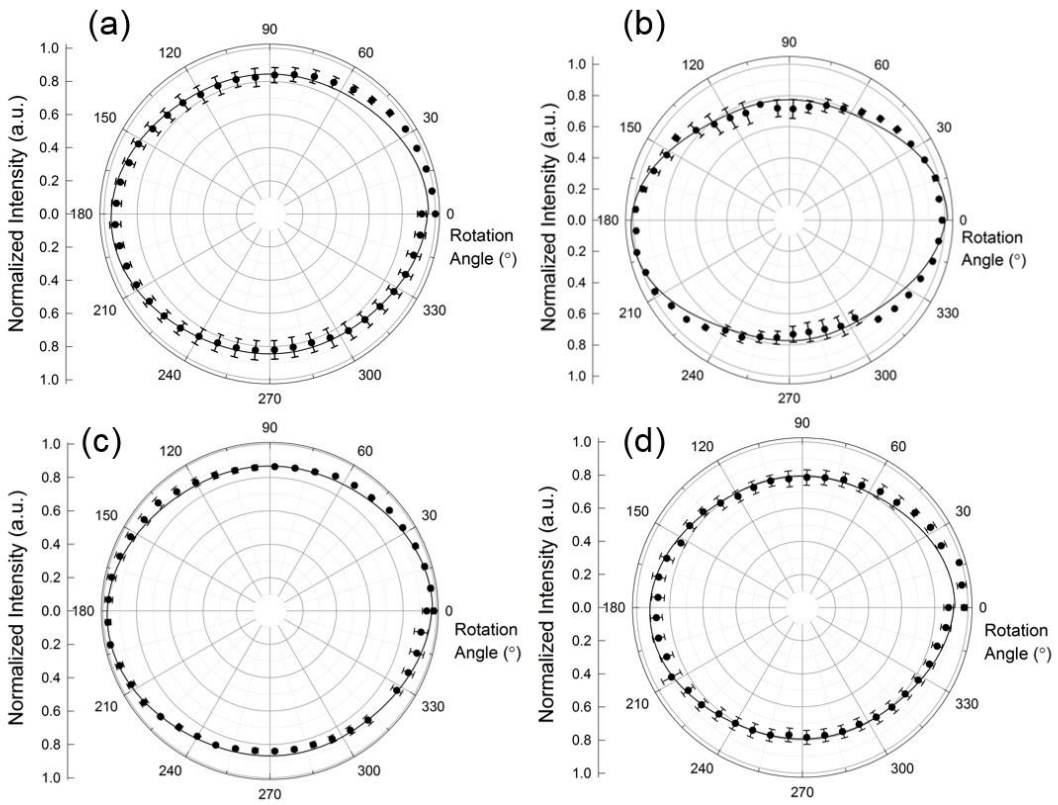

Figure 4. Polar plots of the normalized intensity of the Raman band located at ~1095 cm^{-1} as a function of rotation angle of the polarization with respect to the fibre axis showing the orientation CNCs in composite nanofibres of PS/CNC (a) 10% (b) 20%, and PVA/CNCs (c) 10%, (d) 20%. The solid line represents a fit of $I = r + t * Cos^4\theta$

intensity remained approximately constant with rotation angle for both PS/CNC and PVA/CNC based composite fibres. Previous research has shown that more ellipsoidal shapes are obtained for these polar plots when orientation of the cellulose occurs, be it in chain form or emanating from CNCs [18, 19]. This suggests a lack of orientation of CNCs in both PS and PVA fibres. However, at a higher concentration of CNCs of 20%, both PS/CNC and PVA/CNC fibres appear to exhibit some orientation of the reinforcing phase, as evidenced by the slightly ellipsoidal shape of the data points in the polar plot. The ratio

of the intensity of the band at 90° to the band at 0° ($I_{90°}/I_{0°}$) can be used to characterize the degree of alignment of CNCs along the fibre axis. The values of $I_{90°}/I_{0°}$ are 0.84 and 0.71 for 10% and 20% of CNCs in PS fibres, and $I_{90°}/I_{0°}$ are 0.86 and 0.75 for 10% and 20% CNCs in PVA fibres. These values suggest that both PS/CNC and PVA/CNC fibres with 20% CNCs exhibit a slight orientation of CNCs along the fibre axis direction. These data were fitted using the equation

$$I = r + t * Cos^4\theta \quad (1)$$

where *r* and *t* are fitting parameters, θ is the rotation angle and *I* is the intensity.

The values of these fitting parameters for these polar plots are given in Table 1. Equation 1 has been previously used to fit orientation data for graphene oxide nanocomposites [20].

Table 1. Parameter values for fits of equation to orientation data in Figure 4.

Composite Fibre	**'r'**	**'t'**	**'R^2'**
PS/CNC 10%	0.84	0.11	0.71
PS/CNC 20%	0.77	0.24	0.88
PVA/CNC 10%	0.85	0.09	0.82
PVA/CNC 20%	0.76	0.15	0.74

We acknowledge that misorientation of the fibres could affect the values obtained via Raman spectroscopy. Image analysis was therefore used to calculate the fibre orientation parameter *f* based on the following equation

$$f = \frac{3\langle \cos^2 \theta \rangle - 1}{2} \quad (2)$$

where θ represents the angle between the fibres' axes and the orientation direction; $f = 1$ corresponds to perfect alignment of the fibres, $f = 0$ to a lack of preferred orientation and $f = -1/2$ to perpendicular orientation. Equation 2 has been previously used to assess the orientation of electrospun fibres [21]. We obtained values of 0.94 and 0.95 for PS/CNC 10 and 20 wt.% mats, and 0.94 and 0.67 for PVA/CNC 10 and 20 wt% mats respectively. These values suggest that there is a high degree of orientation of fibres in our fibre mats. We do note however that a value of 0.67 for the 20 wt% sample would suggest some degree of misalignment.

To further elucidate the orientation of CNCs in the fibres, TEM characterization was performed on thin sections of fibres embedded in a supporting matrix. The fibres were sectioned to have a thickness of ~100 nm suitable for viewing in the TEM. Sections were taken along and plane perpendicular to the electrospun fibre axis. CNCs were stained using uranyl acetate before imaging. This staining agent applies a passive outline for CNCs. Several attempts were made to image the PS/CNC fibres using this approach (Figure 5). However, CNCs were not clearly visible in the fibres (darker regions in the fibres suggest their presence), possibly due to lack of contrast between CNCs and PS.

Figure 6 shows a cross-sectional image of a PVA/CNC 10% nanofibre exhibiting clearly randomly oriented CNCs perpendicular to the direction of the fibre axis; a few CNCs were found to be oriented along the fibres' axis (also Figure 6). The aspect ratios of our CNCs have been measured and found to be ~18 (lengths 109 ± 34.5 nm and widths 6.0 ± 1.9 nm) with some variability. It is noted that our electrospun fibres are much wider than the average length of a CNC, and so little protrusion of the CNCs is observed. It is acknowledged that microtoming using a glass knife may have assisted the orientation of CNCs in the cutting direction due to the application of shear forces. If this were the case however, we might have expected to see dominant orientation perpendicular to the fibre axis in one particular direction. This was not observed in the images we obtained. Microtoming was also carried out at room temperature, well below the glass transition of PVA (~88 °C) [22]. Therefore the PVA was thought to be in the glassy state, which, with the supporting epoxy resin, should offer significant resistance to the movement of CNCs within the PVA during the microtoming process. Attempts to microtome fibres at sub-zero temperatures were not successful due to the complete embrittlement of the resin.

Overall, these results combined with Raman spectroscopic results give evidence for a lack of orientation of CNCs along the axis of the fibres. This has been true for both PS/CNC and PVA/CNC fibres regardless of the differences in electrospinning conditions and fibre diameters. Previous work has shown that single-walled carbon nanotubes (SWNTs) can be oriented in electrospun PVA fibres [23–25]. Given that the size of CNCs and SWNTS are similar, it is surprising that orientation is not achieved with the

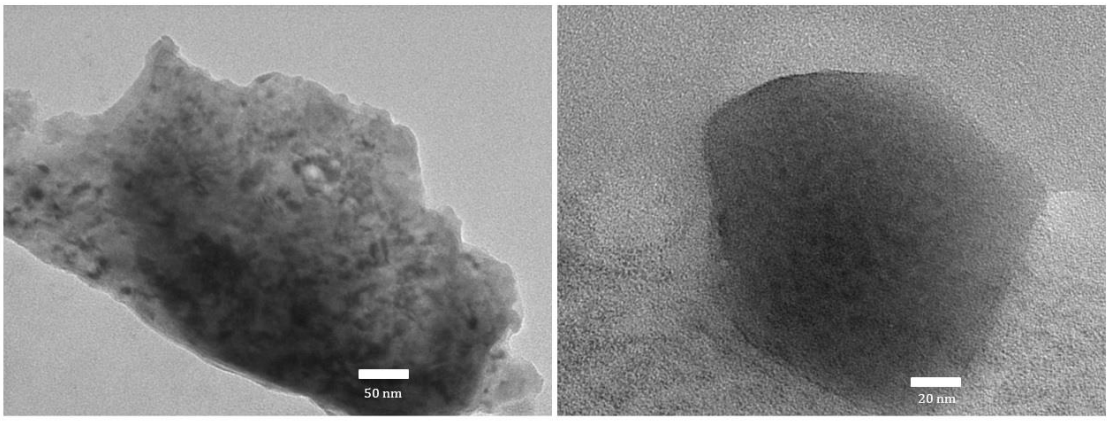

Figure 5 Typical TEM images showing the orientation of CNCs in PS/CNC 10% fibres. Left – image showing CNCs present (darker regions) along the axis of the electrospun fibre, in the plane of the page; Right – image showing CNCs (darker regions) with the axis of the electrospun fibre out of the plane of the page.

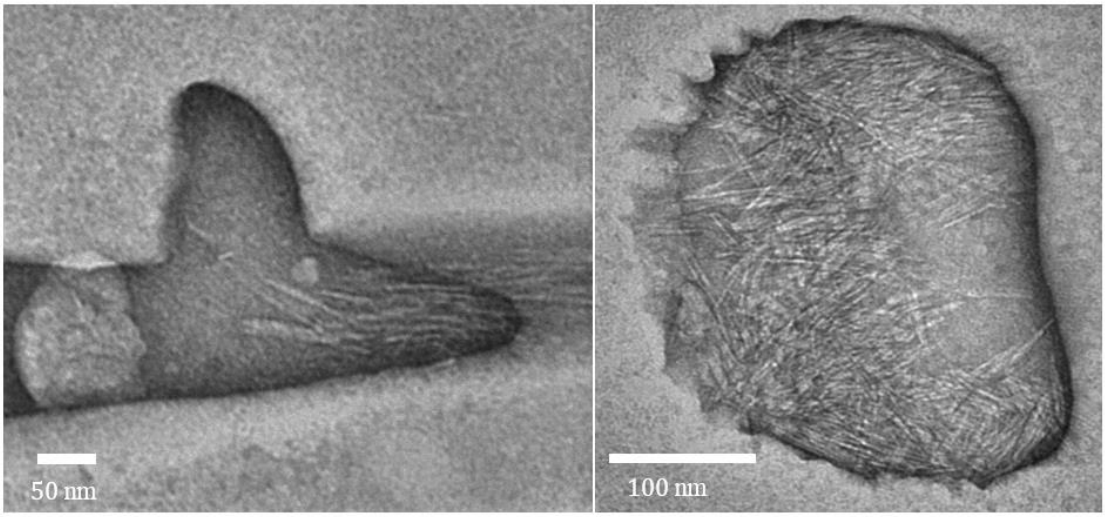

Figure 6. Typical TEM images showing the orientation of CNCs in PVA/CNC 10% fibres. Left – image showing CNCs orientation with the axis of the electrospun fibre in the plane of the page; Right – image showing CNCs orientation with the axis of the electrospun fibre out of the page.

present system. However, different hydrophobic/hydrophilic characteristics of SWNTS and CNCs and their interfacial interactions with the polymer matrix may play a role in dictating orientation. The lack of orientation of CNCs should result in lower axial mechanical properties than would be expected for the electrospun fibres.

3.3. Micromechanical Modeling of Tensile Modulus of Composite Fibres

Tensile moduli of CNC-reinforced composite fibres can be predicted using the rule of mixtures [26] and the Cox model [27]. This model was developed based on the classical shear-lag theory and has been commonly used to predict the tensile moduli of randomly oriented short fibre composites [27]. Several assumptions are required to apply this model to composite fibres; (i) both fibre and matrix undergo elastic deformation, (ii) fibre ends bear no axial loads and (iii) the presence of a fully-bonded fibre-matrix interface [26, 27]. In this case, CNCs are assumed to behave as nanoscale fibres, which are embedded in a polymer matrix to form the larger composite fibres.

The rule of mixtures model, with added efficiency factors (according to Cox), is governed by the equation

$$E_{\text{fibre}} = \eta_{\text{L}} * \eta_{\text{o}}^{\text{CNC}} * E_{\text{CNC}} * V_{\text{CNC}} + E_{\text{polymer}}(1 - V_{\text{CNC}}) \quad (3)$$

where E_{fibre}, η_{L}, η_o^{CNC}, E_{CNC}, V_{CNC}, E_{polymer} represent composite fibre modulus, fibre length efficiency factor (according to Cox theory), orientation factor for CNCs (again according

to Cox), the modulus of the CNCs, CNC volume fraction and the elastic modulus of the polymer matrix, respectively. Equation 3 predicts the modulus of one electrospun fibre with a volume fraction of misoriented CNCs. Electrospun fibre mats that are considered in this study are mostly themselves randomly oriented and therefore modulus of the fibre mat can be calculated by using a fibre orientation factor of 1/3 according to Cox's theory[1]

$$E_{\mathrm{c}} = \eta_{\mathrm{o}}^{\mathrm{fibre}} * E_{\mathrm{fibre}} \quad (4)$$

where E_{c} and $\eta_{\mathrm{o}}^{\mathrm{fibre}}$ are the modulus of the mat and fibre orientation factor, respectively. The orientation factors ($\eta_{\mathrm{o}}^{\mathrm{fibre}}$ or $\eta_{\mathrm{o}}^{\mathrm{CNC}}$) are equal to 1 for highly oriented fibres or CNCs and is taken as 1/3 if either is randomly oriented. It is worth noting that Cox derived his theory [27] for fibrous networks (in this case paper). We note that electrospun networks can be very porous, and perhaps there are fewer interactions between fibres than for a network of hydrogen bonded fibres (for paper). Therefore there could be some influence of the porosity of the networks. Evidence for this comes from the data presented in Table 2 for electrospun fibre networks. Data for single electrospun fibres is scarce in the literature, but one study has reported tensile moduli of ~120 MPa for single PCL fibres [30]. A value of 6 MPa for the PCL networks [6] (it is noted that this value is with fillers) is much lower than 1/3 of 120 MPa (40 MPa) and so it is reasonable to assume that Equation 4 may make some over-prediction of the mat modulus. We have considered two possibilities of fibre arrangement electrospun fibres: (i) fibres are randomly oriented ($\eta_{\mathrm{o}}^{\mathrm{fibre}}$ = 1/3) in the mats and CNCs are perfectly oriented ($\eta_{\mathrm{o}}^{\mathrm{CNC}}$ = 1) along the electrospun

[1] Krenchel [28] uses a factor of $3/8$ - which is close to $1/3$ – for randomly oriented fibres.

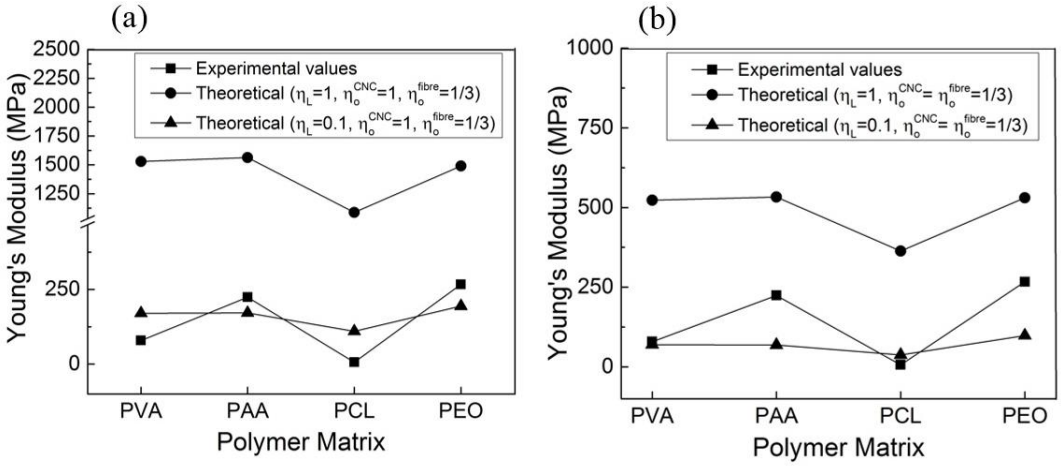

Figure 7. A comparison between experimental and theoretical values of Young's moduli electrospun polymer/CNC fibre mats with different polymeric matrices; (a) only CNCs are highly oriented (η_o=1/3) (b) both fibres and CNCs are randomly oriented. Theoretical values were calculated using the equation (3 and 4). Experimental values were taken from references [6, 8, 17, 29].

fibres' axes (Figure 7a) and (ii) both electrospun fibres and CNCs (within the fibres) are randomly oriented (η_o^{fibre} = 1/3 and η_o^{CNC} = 1/3) (Figure 7b). Upper and lower limits of η_L are considered for the calculation for (i) high aspect ratios nanofibres (η_L=1) and (ii) low aspect ratio nanofibres as η_L=0.1 (an estimate for short fibres [31]). Figures 7a and 7b compare experimental values and theoretical values of Young's moduli for 4 different CNC-reinforced electrospun fibre systems. All experimental Young's moduli values have been obtained from mechanical data reported for electrospun fibre webs (Table 2) [6, 8, 17, 31]. The aspect ratios of the CNCs used for the studies used in this analysis were ~30 for PVA, PAA, PCL, and ~100 for PEO fibres. Further, all electrospun fibres in the studies we focused on were reported to be randomly oriented, except for PEO electrospun fibres;

however, the SEM images presented in this paper [17] show a few unoriented fibres as well. A Young's modulus of the CNCs is taken as 57 GPa [32].

Table 2. Summary of data utilized in the calculation of theoretical moduli

Matrix Polymer	CNC %	Young's Modulus (MPa)	Average Fibre Diameter (nm)	Aspect ratio of CNCs	Reference
PVA	10	89	235	27	[8]
PAA	10	224	141	30	[28]
PCL	7.5	6	200	30*	[6]
PEO	10	267	448	100	[17]

* The reported values of CNC dimensions are 3-10 nm for diameter and 100-250 nm for length.

When modeling, we have considered the possibility that the electrospun fibres and the CNCs can either both be oriented or non-oriented and variants of both. Non-oriented electrospun fibres in a mat, containing oriented low aspect ratio CNCs would give an efficiency factor of 1/3 (and 0.1 for the fibre length efficiency). This is expected to give good agreement between theoretical and experimental data. Indeed this is evidenced by the results shown in Figure 5a. This suggests that CNCs could be oriented within the fibres for all electrospun fibre webs considered in the studies in the literature. Further, we have examined the experimental Young's moduli and theoretical values when both fibres and CNCs are randomly oriented. As expected, for higher aspect ratio fibres (η_L=1), the theoretical values were always higher (Figure 5a) than experimental moduli due to the fact that CNCs typically have low aspect ratios (<100). This was also observed for PEO/CNC

fibres where the CNC aspect ratio was higher (~100). We do note again that Equation 4 could over-predict the modulus of a mat of fibres, due to the influence of significant porosity in the networks. If this is the case then better agreement with the upper set of predicted data in Figure 7 (represented in each case by solid circles) and experimental data is expected.

Further, if we assume that the PEO/CNC fibres are highly oriented (with η_o^{fibre}=1) then the theoretical moduli will be even higher than experimental values. However, when a lower aspect ratio of CNCs (η_L = 0.1) was used, with random orientation of both the CNCs and fibres, there is again agreement with the experimental moduli (Figure 5b). It may therefore be true that low aspect ratio CNCs (such as cotton) remain unoriented in the fibres, in agreement with our own experimental evidence. Overall, these micromechanical modeling data suggests that CNCs could indeed be oriented along the fibre axis direction. It is likely that the real situation will be some way between these two extreme cases, with some misorientation remaining. Indeed we have shown that orientation of the CNCs can occur, although it appears that random orientation can also remain in the fibres. Further work is required to carefully control the spinning procedure therefore to ensure a more uniform orientation.

4. Conclusions

PS and PVA nanofibers containing CNCs were successfully produced by electrospinning. PS/CNC fibres were observed to have larger fibre diameters in the range of ~3 μm when compared to PVA/CNC fibres (~0.3μm). Raman spectroscopic analysis of oriented fibres

within mats showed some evidence for a lack of orientation of CNCs in the polymer fibres. Slightly ellipsoidal shapes to the polar intensity maps and a lower value for the intensity ratio $I_{90°}/I_0$ indicates that CNCs were slightly oriented in polymer fibres with a 20% volume fraction.. TEM images of CNC-reinforced polymer fibres confirmed the random orientation of CNCs in PVA fibres with local regions of oriented CNCs in the cross section and a few CNCs oriented along the axis of the fibre. These data are expected to provide a vital insight into the orientation of CNCs in polymer fibres produced by electrospinning. The strong electric fields and confinement effect associated with electrospinning may not necessarily induce full orientation of CNCs. A comparison of mechanical data from previously published work and theoretical calculations using the rule of mixtures also seems to suggest that this is possibly the case.

Acknowledgement

Authors would like to thank Peter Splatt, College of Life and Environmental Sciences, University of Exeter for assistance in microtoming and staining samples. We also thank Dr. Hong Chang for assistance in TEM imaging. The Engineering and Physical Sciences Research Council (EPSRC) are acknowledged for funding under grant no. EP/L017679/1. We would like to thank Dr. Fenglei Zhou, Materials Science Centre at University of Manchester, UK for assistance with electrospinning.

Conflict of Interest

The authors declare that they have no conflict of interest.

References

1. Qiu X, Hu S (2013) “Smart” materials based on cellulose: A review of the preparations, properties, and applications. Materials 6:738–781.
2. Samir MASA, Dufresne A (2005) Review of Recent Research into Cellulosic Whisker, Their Properties and Their Application in Nanocomposites Field. Biomacromol 6:612–626.
3. Hsieh Y-.L (2013) Cellulose nanocrystals and self-assembled nanostructures from cotton, rice straw and grape skin: A source perspective. J Mater Sci 48:7837–7846.
4. Vallejos ME, Peresin MS, Rojas OJ (2012) All-Cellulose Composite Fibers Obtained by Electrospinning Dispersions of Cellulose Acetate and Cellulose Nanocrystals. J Polym Environ 20:1075–1083.
5. Valentini L, Bittolo Bon S, Fortunati E, Kenny JM (2014) Preparation of transparent and conductive cellulose nanocrystals/graphene nanoplatelets films. J Mater Sci 49:1009–1013.
6. Zoppe JO, Peresin MS, Habibi Y, Venditti RA, Rojas OJ (2009) Reinforcing poly(ε-caprolactone) nanofibers with cellulose nanocrystals. ACS Appl Mater Inter 1:1996–2004.
7. Martínez-Sanz M, Olsson RT, Lopez-Rubio A, Lagaron JM (2011) Development of electrospun EVOH fibres reinforced with bacterial cellulose nanowhiskers. Part I: Characterization and method optimization. Cellulose 18:335–347.
8. Peresin M, Habibi Y, Zoppe JO, Pawlak JJ, Rojas OJ (2010) Nanofiber Composites of Polyvinyl Alcohol and Cellulose Nanocrystals: Manufacture and Characterisation. Biomacromol 11:674–681.

9. Ding B, Kim H-Y, Lee S-C, Lee DR, Choi KJ (2002) Preparation and characterization of nanoscaled poly(vinyl alcohol) fibers via electrospinning. Fiber and Polym 3:73–79.

10. Koski A, Yim K, Shivkumar S (2004) Effect of molecular weight on fibrous PVA produced by electrospinning. Mater. Lett. 58:493–497.

11. Lee HW, Karim MR, Ji HM, Choi JH, Do Ghim H, Park SM, Oh W, Yeum JH (2009) Electrospinning Fabrication and Characterization of Poly (vinyl alcohol)/Montmorillonite Nanofiber Mats. J Appl Polym Sci 113: 1860-1867.

12. Rojas OJ, Montero GA, Habibi Y (2009) Electrospun nanocomposites from polystyrene loaded with cellulose nanowhiskers. J Appl Polym Sci. 113:927–935.

13. Bordel D, Putaux J-L, Heux L (2006) Orientation of native cellulose in an electric field. Langmuir 22:4899–4901.

14. Pullawan T, Wilkinson AN, Eichhorn SJ (2012) Influence of magnetic field alignment of cellulose whiskers on the mechanics of all-cellulose nanocomposites. Biomacromolecules 13:2528–2536.

15. Iwamoto S, Isogai A, Iwata T (2011) Structure and mechanical properties of wet-spun fibers made from natural cellulose nanofibers. Biomacromol 12:831–836.

16. Huang ZM, Zhang YZ, Kotaki M, Ramakrishna S (2003) A review on polymer nanofibers by electrospinning and their applications in nanocomposites. Compos Sci Technol 63:2223–2253

17. Changsarn S, Mendez JD, Shanmuganathan K, Foster EJ, Weder C, Supaphol P (2011) Biologically inspired hierarchical design of nanocomposites based on

poly(ethylene oxide) and cellulose nanofibers. Macromol Rapid Comm 32:1367–1372.

18. Pullawan T, Wilkinson AN, Eichhorn SJ (2013) Orientation and deformation of wet-stretched all-cellulose nanocomposites. J Mater Sci 48:7847–7855.
19. Bakri B, Eichhorn SJ (2010) Elastic coils: deformation micromechanics of coir and celery fibres. Cellulose 17: 1-11.
20. Li Z, Young RJ, Kinloch IA (2013) Interfacial stress transfer in graphene oxide nanocomposites. ACS Appl Mater Inter 5:456–463.
21. Wang M, Yu JH, Kaplan DL, Rutledge GC (2006) Production of Submicron Diameter Silk Fibres Under Benign Processing Conditions by Two-Fluid Electrospinning. Macromolecules 39:1102-1107.
22. Wanasekara ND, Stone DA, Wnek GE, Korley LTJ (2012) Stimuli-Responsive and Mechanically-Switchable Electrospun Composites. Macromolecules 45:9092–9099.
23. Deng L, Young RJ, Sun R, Zhang GP, Lu DQD, Li H, Eichhorn SJ (2014) Unique Identification of Single-Walled Carbon Nanotubes in Electrospun Fibers. J Phys. Chem C, 118:24025–24033.
24. Kannan P, Eichhorn SJ, Young RJ (2007) Deformation of isolated single-wall carbon nanotubes in electrospun polymer nanofibres. Nanotechnology 18:235707.
25. Kannan P, Young RJ, Eichhorn SJ (2008) Debundling, isolation, and identification of carbon nanotubes in electrospun nanofibers. Small 4:930–933.
26. Harris B (1999) Engineering Composite Materials. IOM Communications Ltd (Institute of Materials).

27. Cox HL (1952) The elasticity and strength of paper and other fibrous materials. Brit J Appl Phys 3:72–79.

28. Krenchel H (1964) Fibre Reinforcement. Akademisk Forlag, Copenhagen, Denmark.

29. Lu P, Hsieh Y-L (2009) Cellulose nanocrystal-filled poly(acrylic acid) nanocomposite fibrous membranes. Nanotechnology 20:415604.

30. Tan EPS, Ng SY, Lim CT (2005) Tensile testing of a single ultrafine polymeric fiber. Biomaterials 26:1453-1456.

31. Lee K-Y, Aitomäki Y, Berglund LA, Oksman K, Bismarck A (2014) On the use of nanocellulose as reinforcement in polymer matrix composites. Compos Sci Technol 105:15–27.

32. Rusli R, Eichhorn SJ (2008) Determination of the stiffness of cellulose nanowhiskers and the fiber-matrix interface in a nanocomposite using Raman spectroscopy. Appl Phys Lett 93:1–3.